OPEN

Original article

Nuclear Medicine Communications

Computed tomography–based skeletal segmentation for quantitative PET metrics of bone involvement in multiple myeloma

Maria E.S. Takahashi[a,b], Camila Mosci[c], Edna M. Souza[c,d], Sérgio Q. Brunetto[c,d], Cármino de Souza[a,e], Fernando V. Pericole[e], Irene Lorand-Metze[f] and Celso D. Ramos[a,c]

Purpose **Quantifications in nuclear medicine are occasionally limited by the lack of standardization for defining volumes of interest (VOIs) on functional images. In the present article, we propose the use of computed tomography (CT)–based skeletal segmentation to determine anatomically the VOI in order to calculate quantitative parameters of fluorine 18 *fluorodeoxyglucose* (^{18}F-FDG) PET/CT images from patients with multiple myeloma.**

Methods **We evaluated 101 whole-body ^{18}F-FDG PET/CTs of 58 patients with multiple myeloma. An initial subjective visual analysis of the PET images was used to classify the bone involvement as negative/mild, moderate, or marked. Then, a fully automated CT–based segmentation of the skeleton was performed on PET images. The maximum, mean, and SD of the standardized uptake values (SUV_{max}, SUV_{mean}, and SD_{SUV}) were calculated for bone tissue and compared with the visual analysis.**

Results **Forty-five (44.5%), 32 (31.7%), and 24 (23.8%) PET images were, respectively, classified as negative/mild, moderate, or marked bone involvement. All quantitative parameters were significantly related to the visual assessment of bone involvement. This association was stronger for the SUV_{mean} [odds ratio (OR): 10.52 (95% confidence interval (CI), 5.68–19.48); $P < 0.0001$] and for the SD_{SUV} [OR: 5.58 (95% CI, 3.31–9.42); $P < 0.001$) than for the SUV_{max} [OR: 1.01 (95% CI, 1.003–1.022); $P = 0.003$].**

Conclusion **CT–based skeletal segmentation allows for automated and therefore reproducible calculation of PET quantitative parameters of bone involvement in patients with multiple myeloma. Using this method, the SUV_{mean} and its respective SD correlated better with the visual analysis of ^{18}F-FDG PET images than SUVmax. Its value in staging and evaluating therapy response needs to be evaluated.**
Nucl Med Commun **41: 377–382**

Nuclear Medicine Communications 2020, **41**:377–382

Keywords: bone segmentation, fluorine 18 fluorodeoxyglucose PET/computed tomography, multiple myeloma, standardized uptake values

[a]School of Medical Sciences, [b]Physics Institute, [c]Division of Nuclear Medicine, [d]Center of Biomedical Engineering, [e]Center of Hematology and Hemotherapy and [f]Department of Internal Medicine, Faculty of Medical Sciences, University of Campinas, Campinas, Brazil

Correspondence to Celso Dario Ramos, MD, PhD, Department of Radiology, Division of Nuclear Medicine, University of Campinas, Rua Roxo Moreira s/n, PO Box 6142, 13083-970, Campinas, Brazil
Tel: +55 19 3521 7801; fax: +55 19 3521 7821; e-mail: cdramos@unicamp.br

Received 12 September 2019 **Accepted** 14 January 2020

Introduction

The lack of standardization for segmentation of specific volumes has been an obstacle for metabolic parameters calculation of PET images [1–5] especially for irregular and extensive tissue where manual segmentation is impracticable.

The use of computed tomography (CT) in hybrid nuclear medicine equipments has brought many benefits, like attenuation correction and visual correlation between functional and anatomic images [6–12]. Another advantage that has been explored in recent years is CT–based segmentation of PET images, where a volume of interest (VOI) is determined based on the anatomical contour and not on the patterns of radiopharmaceutical uptake [13–15].

For multiple myeloma, where bone involvement is an important factor for staging and clinical management of the patient [16–20], CT–based bone segmentation of fluorine 18 *fluorodeoxyglucose* (^{18}F-FDG) PET can enable the calculation of parameters that are not yet fully explored.

In this work, we performed a CT–based skeletal segmentation of ^{18}F-FDG PET images to calculate three quantitative parameters of the standardized uptake value (SUV) for bone tissue of patients with multiple myeloma: maximum (SUV_{max}), mean (SUV_{mean}), and standard deviation (SD) of SUV (SD_{SUV}). These parameters were compared with results from visual analysis of bone involvement degree.

0143-3636 Copyright © 2020 The Author(s). Published by Wolters Kluwer Health, Inc. DOI: 10.1097/MNM.0000000000001165

Method

This study was approved by the local ethics committee (CAAE 97966618.5.0000.5404), and written informed consent was waived by the ethics committee. We retrospectively evaluated 101 whole-body ^{18}F-FDG PET/CT examinations from 58 patients with multiple myeloma according to the updated criteria of the International Myeloma Working Group (IMWG) [18] between 2013 and 2018. Twenty-nine of them had the ^{18}F-FDG PET/CT images repeated during follow-up between June 2013 and September 2018. Therefore, 29/58 patients had one, 20/58 had two, 4/58 had three, and 5/58 had four ^{18}F-FDG PET/CT performed during this period of time.

According to the standard protocol for multiple myeloma of our center, the patients were instructed to fast for at least 6 h. Image acquisitions started 60 min after the injection of 0.12 mCi/kg of ^{18}F-FDG. All patients were scanned from head to feet, in a Biography mCT40 PET/CT scanner (Siemens Medical Solutions Inc., Knoxville, Tennessee, USA). The emission scan was performed in a 3D mode, 1.5 min per bed position. PET images were reconstructed using a standard iterative algorithm (ordered subset expectation maximization + point spread function + time-of-flight with 2 iterations and 21 subsets). The CT part of the study was acquired with 120–140 kV, 120 mA, transaxial field of view 700 mm, rotation time 0.8 s, and slice thickness 2.1 mm. CT data were used for attenuation correction and no correction for partial volume effect (PVE) was performed.

Prior to CT–based bone segmentation, a preprocessing was made for exclusion of external objects, like patient table and urinary catheter. Also, areas of normal ^{18}F-FDG uptake (liver, bladder, kidneys, heart, and brain) were also subtracted from original PET to avoid overlapping artifacts. Internal objects in the same Hounsfield unit range as the segmented volume were not excluded unless ^{18}F-FDG uptake could produce a false positive. In this case, manual exclusion was performed.

Bone segmentation was performed in four steps: (1) a CT–based segmentation using a global threshold that corresponded to the compact bone tissue to produce a masked PET image; (2) masked PET conversion to binary image; (3) morphological closing of the binary image; and (4) element-wise multiplication between closed image and original ^{18}F-FDG PET image.

In the first step, we used Hounsfield unit higher than 100 as global threshold. This value was set based on CT-histogram analysis and also visual assessment. All voxels with Hounsfield unit <100 on CT were set to zero on the correspondent masked PET.

Morphological close was made using a structuring element in a disc format with radius equal to 3 pixels. The purpose of morphological close operation was to include the 'soft' portion of the skeleton in the bone mask.

Once segmentation was completed, the following quantitative parameters were calculated exclusively for the entire bone tissue (except skull): maximum SUV (SUV_{max}), mean SUV (SUV_{mean}), and its respective SD (SD_{SUV}). Figure 1 shows a flowchart of this analysis.

CT–based segmentation was performed using the Beth Israel Plugin for Fiji [21,22]. Final bone mask and quantitative metrics calculations were performed with an in-house software implemented in MATLAB, Natick, Massachusetts, USA [23,24].

Global visual analysis of ^{18}F-FDG PET/CT was performed by two experienced nuclear physicians. They classified images as negative when no focal lesion or diffuse

Fig. 1

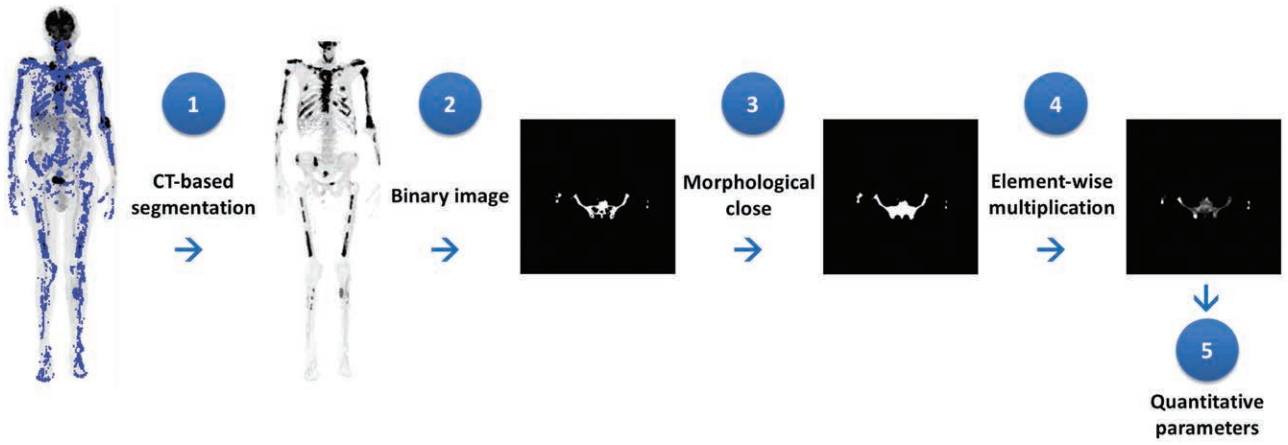

Flowchart for quantitative PET metrics: a CT–based segmentation, masked PET conversion to binary image, morphological closing and element-wise multiplication between closed image and original ^{18}F-FDG PET image, and finally, quantitative metrics calculation. CT, Computed tomography; ^{18}F-FDG PET, fluorine 18 fluorodeoxyglucose PET.

disease was found on ^{18}F-FDG PET/CT examinations. Mild bone involvement was defined when less than five focal lesions or limited/mild diffuse disease was observed on image. Images were classified as moderate bone involvement when 5–20 focal lesions or moderate diffuse disease was observed. Images were classified as presenting marked bone involvement when more than 20 focal lesions or severe diffuse disease was observed [25,26].

We applied the generalized estimating equation (GEE) to the univariate analysis to verify the relation between quantitative parameters and the global visual analysis [27]. Univariate analysis was performed by using the Statistical Analysis *Software* for Windows (SAS Institute Inc, 2002–2008, Cary, North Carolina, USA).

Results

The visual analysis classified 45 of the 101 ^{18}F-FDG PET/CT images (44.5%) as negative or presenting mild bone involvement, 32 (31.7%) as moderate and 24 (23.8%) as marked bone involvement (Fig. 2).

Mean SUV_{max}, mean SUV_{mean}, and mean SD_{SUV} were, respectively: 8.5 ± 6.6, 0.9 ± 0.1, and 0.5 ± 0.1 for images classified as negative or mild bone involvement; 12.8 ± 7.8, 0.9 ± 0.1, and 0.7 ± 0.1 for moderate bone involvement; and 27.8 ± 36.4, 1.2 ± 0.2, and 1.1 ± 0.4 for marked bone involvement (Fig. 3). Univariate statistical analysis using GEE showed that all quantitative parameters for bone tissue were significantly related to visual assessment by nuclear physicians ($P < 0.05$). The odds ratio (OR) for SUV_{max} was 1.01 [(95% confidence interval (CI), 1.003–1.022)]; for SUV_{mean} OR, 10.52 (95% CI, 5.68–19.48); and for SD_{SUV} OR, 5.58 (95% CI, 3.31–9.42).

All mean quantitative parameters for each category, its respective ranges, and results for statistic analysis are described in Table 1.

Discussion

Bone imaging, especially ^{18}FDG PET-CT, has become a mainstay in diagnostic evaluation of multiple myeloma

Fig. 2

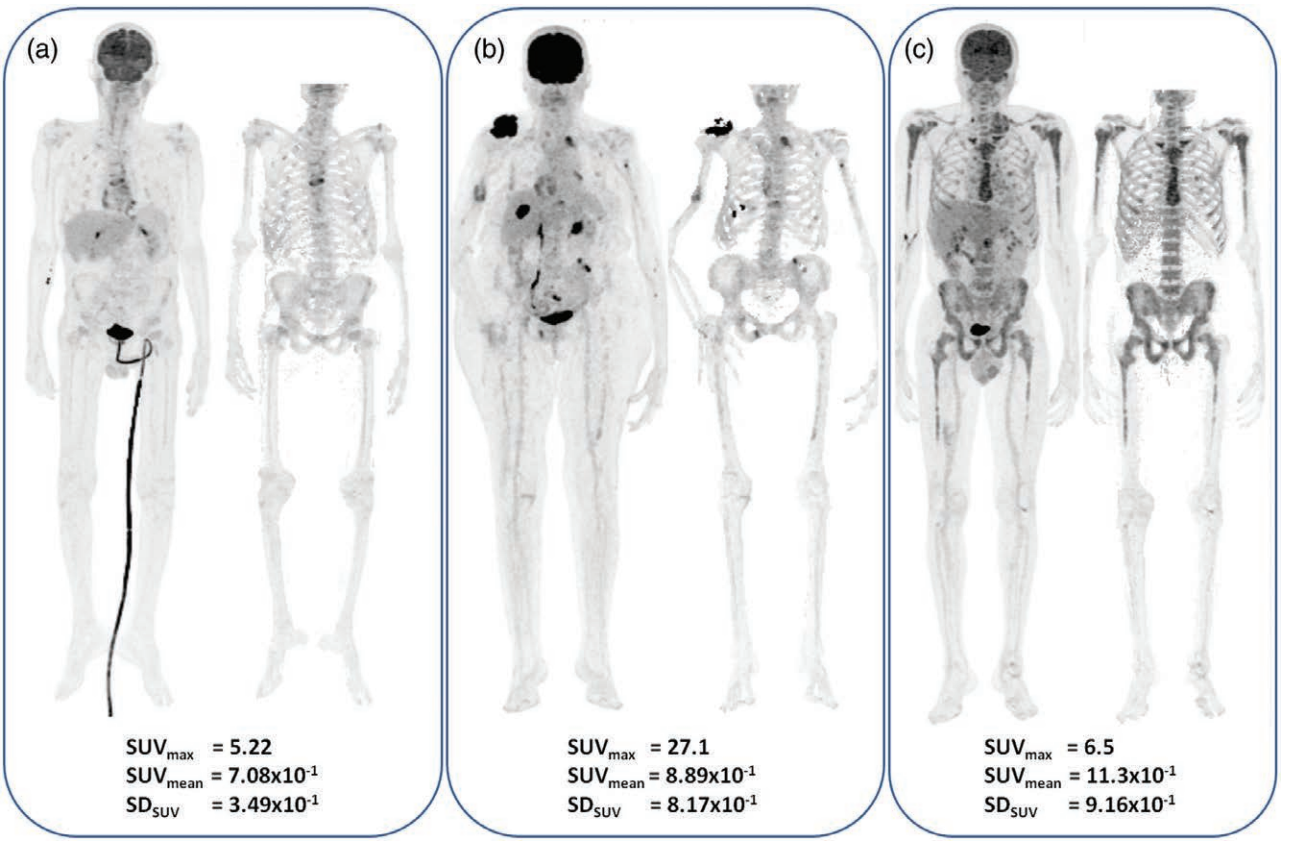

Limitation of maximum SUV (SUV_{max}) as compared with mean SUV (SUVmean) and its SD (SD_{SUV}) for evaluating bone involvement in multiple myeloma SUV_{mean}. (a), (b), and (c) correspond to patients visually classified as presenting mild, moderate, and marked bone involvement, respectively. Their correspondent SUV_{max}, SUV_{mean}, and SD_{SUV} are shown. The point with the highest SUV in each patient is, respectively, the sternum, right shoulder, and clavicle for (a), (b), and (c). Note that, in opposition to SUV_{mean} and SD_{SUV}, SUV_{max} was not able to express the progressive intensity of bone involvement from (a) to (c), as defined by visual analysis. Also note that the proposed method evaluates only the osseous portion of the lesions and does not account for extraosseous extension of the disease, as seen in the left shoulder of the patient in (b). SUV, standardized uptake values; SUV_{max}, maximum SUV; SUV_{mean}, mean SUV; SDsuv, standard deviation of SUV.

Fig. 3

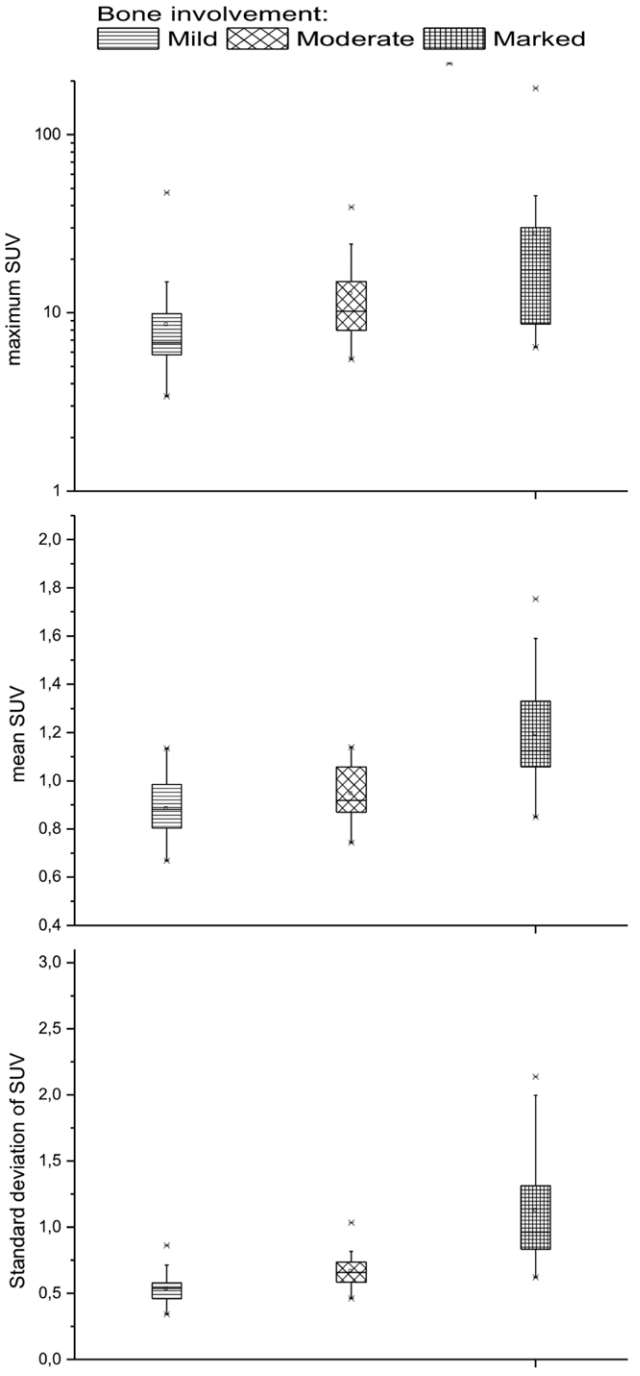

Box plot comparing the three categories of visual assessment of bone involvement for quantitative PET metrics for maximum SUV of bone tissue, mean SUV and SD of SUV. SUV, standardized uptake values.

Table 1 Quantitative parameters of PET/computed tomography for patients with multiple myeloma classified into three groups

Visual assessment of bone involvement	SUV_{max}	SUV_{mean}	SD_{SUV}
Negative or mild			
Mean ± SD	8.5 ± 6.6	$(8.8 \pm 1.3) \times 10^{-1}$	$(5.3 \pm 1.1) \times 10^{-1}$
(Range)	(3.4–47.3)	$(6.7–11.4) \times 10^{-1}$	$(3.4–8.6) \times 10^{-1}$
Moderate			
Mean ± SD	12.8 ± 7.8	$(9.5 \pm 1.1) \times 10^{-1}$	$(6.6 \pm 1.2) \times 10^{-1}$
(Range)	(5.5–39.2)	$(7.4–11.4) \times 10^{-1}$	$(4.6–10.3) \times 10^{-1}$
Marked			
Mean ± SD	27.8 ± 36.4	$(11.9 \pm 2.3) \times 10^{-1}$	$(11.2 \pm 3.9) \times 10^{-1}$
(Range)	(6.4–181.5)	$(8.5–17.5) \times 10^{-1}$	$(6.2–21.4) \times 10^{-1}$
P value	0.0104	<0.0001	< 0.0001
Odds ratio	1.0124	10.5152	5.5837
(95% CI)	(1.0029–1.0219)	(5.6752–19.4828)	(3.3109–9.4166)

Confidence interval, CI; SUV, standardized uptake value.

[28–30]. Besides, it has been used for measuring treatment response and as an important prognostic factor in this disease. However, quantification of bone disease in multiple myeloma has not been fully standardized, and often semiquantitative measures have been used. Several efforts have been made in order to standardize an objective quantitative measure that can be widely reproducible. SUV_{max} has been widely used for many purposes [28,29,31]. The study by Sager *et al.* [29] on bone involvement at initial staging of patients with multiple myeloma found a significant correlation between SUV_{max} and bone marrow cellularity and percentage of plasma cells. Using a multivariate analysis, Zamagni *et al.* [28] found that persistent SUV_{max} above 4.2 after first-line treatment was independently associated with disease progression. Bailly *et al.* [31] proposed SUV_{max} reduction (ΔSUV_{max}) as a powerful tool for the prediction of long-term outcome in patients with FDG-avid multiple myeloma.

On the other hand, the intrinsic limitation of analyzing SUV_{max} as a single voxel with largest intensity is well known and it is evident in Fig. 2. Segmenting only both femurs, Ak and Gulbas [30] calculated the SUV_{mean} of patients with multiple myeloma and found that they were negatively correlated with serum albumin levels of the patients. The CT–based segmentation of the whole skeleton described here may allow a routine use of SUV_{mean} and SD_{SUV}, being reproducible and more robust than SUV_{max}. These parameters could be used to compare different patients and treatments and to access patients' outcome.

Some studies have reported evaluation of the metabolic activity of bone tissue using total or partial segmentation of the skeleton [32–35]. Leydon *et al.* [32] calculated SUV_{mean} in specific regions such as femur, iliac crest, lumbar spine, and sternum for patients with and without chemotherapy, using a CT–based segmentation as one of the steps of image analysis. Nguyen *et al.* [33] also made partial segmentation of the skeleton to assess hematopoietic tissue proliferation on the corresponding vertebral body volume on PET. Mean and maximum SUVs for L1, L3, and L5 of lumbar spine were calculated by Basu *et al.* [35] for five patients with negative FDG PET/CT using MRI-based segmentation. Partial and total skeleton segmentation was executed by Sambuceti *et al.* [34] to measure the metabolic activity of the bone marrow on FDG PET/CT, and they found a mean SUV of intraosseous

space equal to 0.96 ± 0.17 for 35 patients with nonmetastatic melanoma.

Differently from the studies mentioned above, in the present study, we correlated quantitative parameters for whole skeleton with clinical evaluation of the image. We used CT–based segmentation as a tool to calculate three quantitative parameters exclusively for the entire bone tissue for patients with multiple myeloma: SUV_{max}, SUV_{mean}, and SD_{SUV}. Interestingly, SUV_{mean} was the parameter that correlated best with the visual analysis, followed by the SD_{SUV}. This feature can give a good measure of the overall bone involvement in multiple myeloma. Both are first-order texture parameters [36], and in this specific case, they cannot be obtained without bone segmentation.

An important limitation of our method is the need to exclude patient's skull. Normal ^{18}F-FDG brain uptake causes artifacts, generated as 'false-positive' areas of skull uptake. The same limitation was described by Sambuceti *et al.* [34]. Another expected limitation of the approach proposed in the present study is that information about extramedullary lesions or soft tissue involvement is neglected and should be evaluated separately. This also occurs with lesions that exceed the bone limits, since the mathematical index represents only the osseous portion of the lesions.

It is possible that the quantitative parameters studied here may be greatly influenced by PVE, which is known to be an important factor in PET quantification. However, the application of PVE correction in ^{18}F-FDG PET/CT is not yet established, especially for nonbrain studies. Also, PVE correction is unavailable in commercial systems [37–40].

Some artifacts intrinsic of CT–based segmentation may affect quantitative PET imaging parameters as well as bone contour and need special attention, such as metal implants, urinary catheter, and normal 'nonbone' ^{18}F-FDG uptake overlapping the segmented VOI [41]. In these cases, manual subtraction or manual correction of these artifacts should be performed.

Conclusion

CT-based skeletal segmentation can be used to calculate reproducible quantitative parameters for patients with multiple myeloma. Using this method, SUV_{mean} and its respective SD correlated better with the visual analysis of ^{18}F-FDG-PET images than SUV_{max}.

Acknowledgements

The authors would like to thank the Nuclear and Energy Research Institute (IPEN-CNEN), São Paulo, Brazil, for supplying the radiopharmaceuticals used in the present project (IPEN/UNICAMP agreement No. 01342000458/2017-15). The authors are grateful for the financial support from FAPESP (Fundação de Amparo a Pesquisa do Estado de São Paulo), grant numbers 2009/54065-0 and 2018/00654-4.

Conflicts of interest

There are no conflicts of interest.

References

1 Zijlstra JM, Boellaard R. Baseline PET as prognostic marker for Hodgkin? *Blood* 2018; **131**:3–4.
2 Cottereau AS, Buvat I, Kanoun S, Versari A, Casasnovas O, Chauvie S, *et al*. Is there an optimal method for measuring baseline metabolic tumor volume in diffuse large B cell lymphoma? *Eur J Nucl Med Mol Imaging* 2018; **45**:1463–1464.
3 Kanoun S, Tal I, Berriolo-Riedinger A, Rossi C, Riedinger JM, Vrigneaud JM, *et al*. Influence of software tool and methodological aspects of total metabolic tumor volume calculation on baseline [18F]FDG PET to predict survival in Hodgkin lymphoma. *PLoS One* 2015; **10**:e0140830.
4 Hatt M, Tixier F, Pierce L, Kinahan PE, Le Rest CC, Visvikis D. Characterization of PET/CT images using texture analysis: the past, the present… any future? *Eur J Nucl Med Mol Imaging* 2017; **44**:151–165.
5 Leijenaar RT, Nalbantov G, Carvalho S, van Elmpt WJ, Troost EG, Boellaard R, *et al*. The effect of SUV discretization in quantitative FDG-PET radiomics: the need for standardized methodology in tumor texture analysis. *Sci Rep* 2015;**5**:11075.
6 Kinahan PE, Townsend DW, Beyer T, Sashin D. Attenuation correction for a combined 3D PET/CT scanner. *Med Phys* 1998; **25**:2046–2053.
7 Beyer T, Townsend DW, Brun T, Kinahan PE, Charron M, Roddy R, *et al*. A combined PET/CT scanner for clinical oncology. *J Nucl Med* 2000; **41**:1369–1379.
8 Burger C, Goerres G, Schoenes S, Buck A, Lonn AH, Von Schulthess GK. PET attenuation coefficients from CT images: experimental evaluation of the transformation of CT into PET 511-kev attenuation coefficients. *Eur J Nucl Med Mol Imaging* 2002; **29**:922–927.
9 Bar-Shalom R, Yefremov N, Guralnik L, Gaitini D, Frenkel A, Kuten A, *et al*. Clinical performance of PET/CT in evaluation of cancer: additional value for diagnostic imaging and patient management. *J Nucl Med* 2003; **44**:1200–1209.
10 Even-Sapir E, Keidar Z, Bar-Shalom R. Hybrid imaging (SPECT/CT and PET/CT)–improving the diagnostic accuracy of functional/metabolic and anatomic imaging. *Semin Nucl Med* 2009; **39**:264–275.
11 Keidar Z, Israel O, Krausz Y. SPECT/CT in tumor imaging: technical aspects and clinical applications. *Semin Nucl Med* 2003; **33**:205–218.
12 Schillaci O. Hybrid SPECT/CT: a new era for SPECT imaging? *Eur J Nucl Med Mol Imaging* 2005; **32**:521–524.
13 Gutte H, Jakobsson D, Olofsson F, Ohlsson M, Valind S, Loft A, *et al*. Automated interpretation of PET/CT images in patients with lung cancer. *Nucl Med Commun* 2007; **28**:79–84.
14 Al-Zaghal A, Yellanki DP, Ayubcha C, Werner TJ, Høilund-Carlsen PF, Alavi A. CT-based tissue segmentation to assess knee joint inflammation and reactive bone formation assessed by 18F-FDG and 18F-naf PET/CT: effects of age and BMI. *Hell J Nucl Med* 2018; **21**:102–107.
15 Lindgren Belal S, Sadik M, Kaboteh R, Enqvist O, Ulén J, Poulsen MH, *et al*. Deep learning for segmentation of 49 selected bones in CT scans: first step in automated PET/CT-based 3D quantification of skeletal metastases. *Eur J Radiol* 2019; **113**:89–95.
16 Umeda M, Adachi Y, Tomiyama J, Takasaki M, Shin K, Mori M, *et al*.; Society for Geriatric Hematology. [Bone lesions in elderly multiple myeloma]. *Nihon Ronen Igakkai Zasshi* 2002; **39**:631–638.
17 Roodman GD; Multiple Myeloma Research Foundation. Myeloma bone disease: pathogenesis and treatment. *Oncology (Williston Park)* 2005; **19**:983–4, 986.
18 Rajkumar SV, Dimopoulos MA, Palumbo A, Blade J, Merlini G, Mateos MV, *et al*. International myeloma working group updated criteria for the diagnosis of multiple myeloma. *Lancet Oncol* 2014; **15**:e538–e548.
19 Cavo M, Terpos E, Nanni C, Moreau P, Lentzsch S, Zweegman S, *et al*. Role of 18F-FDG PET/CT in the diagnosis and management of multiple myeloma and other plasma cell disorders: a consensus statement by the international myeloma working group. *Lancet Oncol* 2017; **18**:e206–e217.
20 Mesguich C, Fardanesh R, Tanenbaum L, Chari A, Jagannath S, Kostakoglu L. State of the art imaging of multiple myeloma: comparative review of FDG PET/CT imaging in various clinical settings. *Eur J Radiol* 2014; **83**:2203–2223.

21 Schindelin J, Arganda-Carreras I, Frise E, Kaynig V, Longair M, Pietzsch T, *et al*. Fiji: an open-source platform for biological-image analysis. *Nat Methods* 2012; **9**:676–682.

22 Cypess AM, Lehman S, Williams G, Tal I, Rodman D, Goldfine AB, *et al*. Identification and importance of brown adipose tissue in adult humans. *N Engl J Med* 2009; **360**:1509–1517.

23 Thompson CM, Shure L. Image processing toolbox: User's guide: The MartWorks; 1995.

24 Gonzalez RC, Woods RE, Eddins SL. *Digital Image Processing using MATLAB®*. 2nd ed. United States: Gatesmark Publishing; 2009. p. 826.

25 Durie BG, Kyle RA, Belch A, Bensinger W, Blade J, Boccadoro M, *et al*.; Scientific Advisors of the International Myeloma Foundation. Myeloma management guidelines: a consensus report from the scientific advisors of the international myeloma foundation. *Hematol J* 2003; **4**:379–398.

26 Durie BG, Waxman AD, D'Agnolo A, Williams CM. Whole-body (18)F-FDG PET identifies high-risk myeloma. *J Nucl Med* 2002; **43**: 1457–1463.

27 Liang K, Zeger S. Longitudinal data-analysis using generalized linear-models. *Biometrika* 1986; **73**:13–22.

28 Zamagni E, Nanni C, Mancuso K, Tacchetti P, Pezzi A, Pantani L, *et al*. PET/CT improves the definition of complete response and allows to detect otherwise unidentifiable skeletal progression in multiple myeloma. *Clin Cancer Res* 2015; **21**:4384–4390.

29 Sager S, Ergül N, Ciftci H, Cetin G, Güner SI, Cermik TF. The value of FDG PET/CT in the initial staging and bone marrow involvement of patients with multiple myeloma. *Skeletal Radiol* 2011; **40**:843–847.

30 Ak I, Gulbas Z. F-18 FDG uptake of bone marrow on PET/CT scan: it's correlation with CD38/CD138 expressing myeloma cells in bone marrow of patients with multiple myeloma. *Ann Hematol* 2011; **90**:81–87.

31 Bailly C, Carlier T, Jamet B, Eugene T, Touzeau C, Attal M, *et al*. Interim PET analysis in first-line therapy of multiple myeloma: prognostic value of δSUVmax in the FDG-avid patients of the IMAJEM study. *Clin Cancer Res* 2018; **24**:5219–5224.

32 Leydon P, O'Connell M, Greene D, Curran K, editors. *Semi-automatic Bone Marrow Evaluation in PETCT for Multiple Myeloma. Medical Image Understanding and Analysis*. Cham: Springer International Publishing; 2017.

33 Nguyen C, Havlicek J, Duong Q, Vesely S, Gress R, Lindenberg L, *et al*. An automatic 3D CT/PET segmentation framework for bone marrow proliferation assessment. *Proc Int Conf Image Proc* 2016; **2016**:4126–4130.

34 Sambuceti G, Brignone M, Marini C, Massollo M, Fiz F, Morbelli S, *et al*. Estimating the whole bone-marrow asset in humans by a computational approach to integrated PET/CT imaging. *Eur J Nucl Med Mol Imaging* 2012; **39**:1326–1338.

35 Basu S, Houseni M, Bural G, Chamroonat W, Udupa J, Mishra S, Alavi A. Magnetic resonance imaging based bone marrow segmentation for quantitative calculation of pure red marrow metabolism using 2-deoxy-2-[F-18]fluoro-D-glucose-positron emission tomography: a novel application with significant implications for combined structure-function approach. *Mol Imaging Biol* 2007; **9**:361–365.

36 Cook GJR, Siddique M, Taylor BP, Yip C, Chicklore S, Goh V. Radiomics in PET: principles and applications. *Clinical and Translational Imaging*. 2014; **2**:269–276.

37 Zaidi H, Karakatsanis N. Towards enhanced PET quantification in clinical oncology. *Br J Radiol* 2018; **91**:20170508.

38 Hoetjes NJ, van Velden FH, Hoekstra OS, Hoekstra CJ, Krak NC, Lammertsma AA, Boellaard R. Partial volume correction strategies for quantitative FDG PET in oncology. *Eur J Nucl Med Mol Imaging* 2010; **37**:1679–1687.

39 Cysouw MCF, Kramer GM, Hoekstra OS, Frings V, de Langen AJ, Smit EF, *et al*. Accuracy and precision of partial-volume correction in oncological PET/CT studies. *J Nucl Med* 2016; **57**:1642–1649.

40 Cysouw MCF, Kramer GM, Schoonmade LJ, Boellaard R, de Vet HCW, Hoekstra OS. Impact of partial-volume correction in oncological PET studies: a systematic review and meta-analysis. *Eur J Nucl Med Mol Imaging* 2017; **44**:2105–2116.

41 Takahashi MES, Mosci C, Souza EM, Brunetto SQ, Etchebehere E, Santos AO, *et al*. Proposal for a quantitative 18F-FDG PET/CT metabolic parameter to assess the intensity of bone involvement in multiple myeloma. *Sci Rep* 2019; **9**:16429.